PNAS RESEARCH ARTICLE | EARTH, ATMOSPHERIC, AND PLANETARY SCIENCES

Chert oxygen isotope ratios are driven by Earth's thermal evolution

M. Tatzel[a,b,1,2], P. J. Frings[b,c,1], M. Oelze[b,d], D. Herwartz[e], N. K. Lünsdorf[a], and M. Wiedenbeck[f]

Edited by Mark Thiemens, University of California, San Diego, La Jolla, CA; received July 29, 2022; accepted November 11, 2022

The $^{18}O/^{16}O$ ratio of cherts ($\delta^{18}O_{chert}$) increases nearly monotonically by ~15‰ from the Archean to present. Two end-member explanations have emerged: cooling seawater temperature (T_{SW}) and increasing seawater $\delta^{18}O$ ($\delta^{18}O_{sw}$). Yet despite decades of work, there is no consensus, leading some to view the $\delta^{18}O_{chert}$ record as pervasively altered. Here, we demonstrate that cherts are a robust archive of diagenetic temperatures, despite metamorphism and exposure to meteoric fluids, and show that the timing and temperature of quartz precipitation and thus $\delta^{18}O_{chert}$ are determined by the kinetics of silica diagenesis. A diagenetic model shows that $\delta^{18}O_{chert}$ is influenced by heat flow through the sediment column. Heat flow has decreased over time as planetary heat is dissipated, and reasonable Archean-modern heat flow changes account for ~5‰ of the increase in $\delta^{18}O_{chert}$, obviating the need for extreme T_{SW} or $\delta^{18}O_{sw}$ reconstructions. The seawater oxygen isotope budget is also influenced by solid Earth cooling, with a recent reconstruction placing Archean $\delta^{18}O_{SW}$ 5 to 10‰ lower than today. Together, this provides an internally consistent view of the $\delta^{18}O_{chert}$ record as driven by solid Earth cooling over billion-year timescales that is compatible with Precambrian glaciations and biological constraints and satisfyingly accounts for the monotonic nature of the $\delta^{18}O_{chert}$ trend.

oxygen isotopes | silica diagenesis | early Earth | heat flow | climate

Significance

Throughout Earth history, chemical sediments show an enigmatic increase in their $^{18}O/^{16}O$ isotope ratios ($\delta^{18}O$) of ~15‰. This has been interpreted as evidence for either very hot (>70 °C) or very ^{18}O-depleted early oceans. But both of these scenarios are hard to reconcile with other geological and geochemical evidence. Focusing on chert, we show that heat flow through the sediment column controls the rate of diagenetic transformations and thereby the $\delta^{18}O$ of chert. This previously unaccounted for control explains ~5‰ of the increase in chert $\delta^{18}O$ as the solid Earth has cooled and implies only moderately ^{18}O-depleted oceans with a temperate–moderate climate on the early Earth.

The oxygen isotope ratios of cherts ($\delta^{18}O_{chert}$) increase from about 17‰ (SMOW, standard mean ocean water) in the Archean to 32‰ in the Cenozoic with no apparent trend in the range of $\delta^{18}O_{chert}$ values (Fig. 1). Oxygen isotope fractionation between silica and its surrounding fluid is temperature dependent (1), so the face-value interpretation of the $\delta^{18}O_{chert}$ record is decreasing seawater temperatures (T_{sw}) through geologic time (2–8). Reconstructions based on maximum $\delta^{18}O$ values, i.e., samples assumed to have undergone the least diagenetic alteration, yield high Archean T_{sw} of >70 °C (5, 9), conditions under which only the hardiest cyanobacteria could survive (10). Similar reconstructions for the Paleozoic yield T_{sw} of 45 °C, well above the metazoan thermal limit (10, 11). These temperatures are also inconsistent with the occurrence of Proterozoic and Archean glaciations, and the near-monotonic $\delta^{18}O_{chert}$ trend is hard to reconcile with climate cyclicities on tectonic timescales.

The most popular alternative explanation for the $\delta^{18}O_{chert}$ trend invokes lower $\delta^{18}O$ of seawater ($\delta^{18}O_{sw}$) in the distant past (12–15) but is contested on the grounds that continental weathering and hydrothermal alteration of oceanic crust may act to buffer $\delta^{18}O_{sw}$ within a narrow range (16–20) and by near-modern Precambrian $\delta^{18}O_{SW}$ reconstructions from hydrothermally altered rocks (21). Very low $\delta^{18}O_{sw}$ requires an order-of-magnitude change in the ratio of high- to low-temperature water–rock interaction/alteration (22), with implications for the evolution of the Earth system beyond paleoclimate (14, 22).

Secondary alteration, especially through an interaction with meteoric water, has been suggested to account for the $\delta^{18}O_{chert}$ trend (3, 23, 24), implying that almost all samples in the geological record are altered. While this explanation could explain triple oxygen isotope ($\Delta'^{17}O$) deviations from equilibrium with modern seawater (25), recent work demonstrates that chert $\Delta'^{17}O$-offsets can emerge without meteoric alteration (26) and that at least Archean $\Delta'^{17}O_{SW}$ may significantly differ from today's composition (22). Moreover, the alteration hypothesis is difficult to reconcile with the near-monotonic nature of the $\delta^{18}O_{chert}$ trend that requires a linear scaling of the degree of alteration with age, which is inconsistent with the diversity of tectonic histories. Given the increasing recognition that $\delta^{18}O_{chert}$ reflects diagenetic (26, 27)—rather than seawater—temperatures, we explore here the factors that influence silica diagenesis and their effect on $\delta^{18}O_{chert}$ and reevaluate the increase in $\delta^{18}O_{chert}$ over geological time.

Chert—a diagenetic, monomineralic rock composed of microcrystalline quartz—forms via a sequence of stepwise transformations that convert amorphous silica (disordered $SiO_2{\cdot}nH_2O$; opal-A) to quartz. These reactions occur by dissolution–reprecipitation (28)

Author contributions: M.T., P.J.F., and M.O. designed research; M.T., P.J.F., and M.O. performed research; D.H., N.K.L., and M.W. analyzed data; M.T. collected samples; P.J.F. created model; and M.T. and P.J.F. wrote the paper.

The authors declare no competing interest.

This article is a PNAS Direct Submission.

[1]M.T. and P.J.F. contributed equally to this work.

[2]To whom correspondence may be addressed. Email: michael.tatzel@uni-goettingen.de.

This article contains supporting information online at https://www.pnas.org/lookup/suppl/doi:10.1073/pnas.2213076119/-/DCSupplemental.

Published December 14, 2022.

via an intermediate phase of mixed cristobalite/tridymite (opal-CT). The opal-A/opal-CT and opal-CT/quartz transformations tend to occur over relatively narrow depth windows (29) and are associated with a resetting of $\delta^{18}O$ to values equilibrated with local porewaters (27, 30). Extremely low solid-state oxygen isotope diffusion coefficients (31) suggest $\delta^{18}O_{chert}$ is insensitive to alteration. It follows that $\delta^{18}O_{chert}$ is controlled by the conditions under which the quartz precipitated. The most important controls are thus in situ porewater $\delta^{18}O$ and ambient temperatures at the depth of transformation.

The suite of parameters that govern solubilities and transformation kinetics of the three silica phases during burial include the temperature–time (T–t) path sediment follows (32, 33) and sediment geochemistry (34–36). For example, detrital minerals—especially aluminosilicates—are known to alter the solubilities and the crystallographic order of silica phases (28, 34, 37, 38) and possibly the kinetic constants of the dissolution and reprecipitation reactions (34, 36). We use samples from a Neoproterozoic–Cambrian section that have a large range of detrital aluminosilicate abundance (f_{sil}) to demonstrate that $\delta^{18}O$ in authigenic quartz varies systematically with f_{sil} , documenting that variations in the rate of silica transformation—and hence $\delta^{18}O_{chert}$—are dominantly controlled by the kinetics of silica diagenesis and less by seawater temperatures. We develop a silica diagenesis model that uses the kinetics of silica phase transformations to show that part of the $\delta^{18}O_{chert}$ increase over Earth history results from declining heat flow from the solid Earth. The effect of heat flow on $\delta^{18}O_{chert}$ has thus far been overlooked but drastically relaxes the required changes in seawater $\delta^{18}O$ and/or seawater temperature.

Results

Kinetic Controls on Diagenetic Temperatures Recorded in Chert $\delta^{18}O$. To explore the dependence of $\delta^{18}O_{chert}$ on silica transformation kinetics, we investigated the covariation between authigenic quartz $\delta^{18}O$ ($\delta^{18}O_{a\text{-}qtz}$) and f_{sil} in cherts and silicified shales from the 550- to 525-Ma-old (39) Lijiatuo section in South China. The bulk $\delta^{18}O$ values vary between 12.6 and 24.0‰, and f_{sil} ranges from 1 to 70 wt% across the ca. 140-m stratigraphic section. Calculated median $\delta^{18}O_{a\text{-}qtz}$ values (derived via mass balance; *SI Appendix*, Supporting Information 1) range from 12.6 to 28.7‰ and covary with f_{sil} (trend in Fig. 2*A*; $r^2 = 0.56$ and $P < 0.01$). Secondary Ion Mass Spectrometry (SIMS) analyses of microcrystalline quartz confirm their high $\delta^{18}O$ in detrital-rich samples; low and intermediate $\delta^{18}O$ values represent pure or partially overgrown detrital quartz grains (*SI Appendix*, Supporting Information 1 and Fig. 2*A*). Using the temperature–fractionation calibration of Sharp et al. (1) and assuming porewater $\delta^{18}O = -1.1$‰ yields temperatures of 58 °C to 189 °C. Both the absolute values and the range of temperatures are implausible for seawater. Alteration with meteoric water or reequilibration with fluids at elevated temperatures could shift $\delta^{18}O$ to lower values but cannot explain the dependence of $\delta^{18}O_{a\text{-}qtz}$ on f_{sil} . Instead, the data are best explained by a change in the rates of silica polymorph transformation during diagenesis, such that quartz precipitates earlier at higher f_{sil} . This follows the long-standing interpretation of silica polymorph distributions in the Californian Monterey Formation, where the opal-CT/quartz transformation occurs at shallower burial depth and lower temperatures as f_{sil} increases (34). The underlying mechanism is thought to be reduced silica solubility at high f_{sil} that causes higher initial crystallinity in the intermediate opal-CT, such that the time required for crystallographic ordering before transformation to quartz is reduced (34). In summary, the covariation of $\delta^{18}O_{a\text{-}qtz}$ with f_{sil} confirms that $\delta^{18}O_{chert}$ is predominantly controlled by the suite of parameters that determine the kinetics of silica diagenesis and thereby the temperature and timing of the final silica phase transformation.

Lijiatuo section $\delta^{18}O_{a\text{-}qtz}$-inferred temperatures do not correlate with age (as proxied by height in the profile) and are much lower than peak diagenetic temperatures, estimated by Raman spectra of carbonaceous material to ~280 °C (Fig. 2*B*; *Materials and Methods*). Our data thus extend, by >500 Ma, the observation from the Miocene Monterey Formation sediments that $\delta^{18}O_{a\text{-}qtz}$ remains unchanged following quartz formation (30). The preservation of the $\delta^{18}O_{a\text{-}qtz}$–$f_{sil}$ relationship testifies to a pristine $\delta^{18}O_{chert}$ signature set during the final opal-CT/quartz transformation—despite later higher-grade diagenesis and the potential for modern alteration. This observation emphasizes the robustness of $\delta^{18}O_{chert}$ as a recorder of diagenetic conditions in sedimentary cherts and further stresses the importance of transformation kinetics and the prograde T–t pathway in setting $\delta^{18}O_{chert}$.

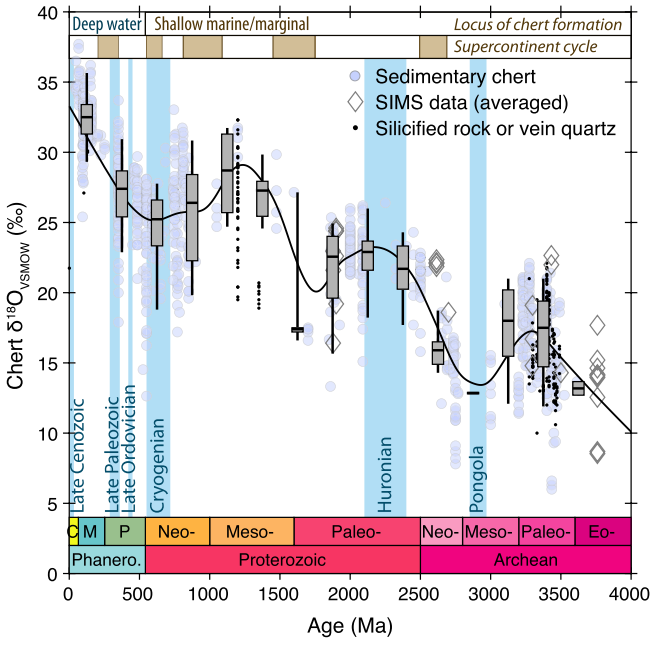

Fig. 1. An updated compilation of oxygen isotope ratios in bulk analyses of sedimentary cherts (*Materials and Methods*). Silicified rocks or quartz veins, along with formation-averaged SIMS data, are plotted but not used to derive the trend. Vertical blue shading indicates periods of inferred low-latitude glaciation. Median $\delta^{18}O_{chert}$ values in 250-Myr-age bins (box-and-whisker plots; center line: median and box limits: upper and lower quartiles) increase by 15‰ from the Paleoarchean to late Phanerozoic, with no apparent trend in the range of $\delta^{18}O_{chert}$ values through time.

Incorporating Silica Transformation Kinetics into a Diagenetic Model. We have developed a 1D reaction–advection–diffusion model to describe the diagenesis of silica polymorphs (full details in *Materials and Methods* and *SI Appendix*, Supporting Information 2). At the heart of the model is a Si mass balance, which couples the dissolution and precipitation of three silica polymorphs (opal-A, opal-CT, and quartz) through a porewater nexus. In the model, opal-A is deposited onto an accumulating sediment column and progressively transforms to opal-CT and quartz as depth and temperature increase. The rates of SiO_2 polymorph dissolution and reprecipitation are governed by kinetic rate constants and the degree of local porewater under- or oversaturation with respect to each phase. Temperature sets the magnitude of oxygen isotope fractionation and influences diagenetic transformation rates via Arrhenius formulations of the kinetic constants of dissolution and reprecipitation. Temperature also influences the solubilities

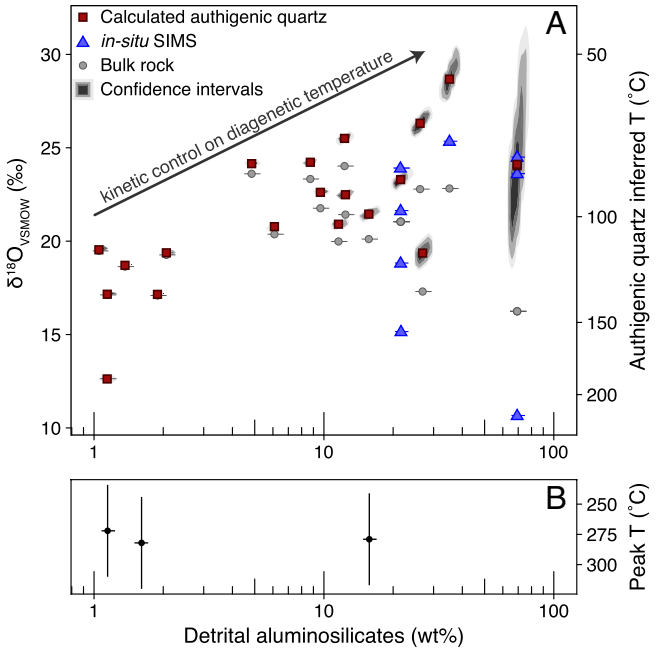

Fig. 2. Oxygen isotope ratios and calculated diagenetic temperatures in cherts and siliceous shales of the Lijiatuo section, China. (*A*) Measured bulk rock $\delta^{18}O$, calculated $\delta^{18}O$ range of authigenic quartz (shading = 50th, 80th, and 95th percentiles) based on Monte Carlo simulations assuming $\delta^{18}O$ of detrital quartz = 9 to 11‰, $\delta^{18}O$ of illite = 15 to 17‰, and illite–detrital quartz ratio from 1.5 to 2.2 (*SI Appendix*, Supporting Information 1), and SIMS $\delta^{18}O$ of individual quartz grains (blue triangles; uncertainties on $\delta^{18}O$ are smaller than the symbol size). The right-hand axis shows corresponding temperatures of quartz formation, assuming a fluid $\delta^{18}O$ of −1.1‰ and using the temperature/oxygen isotope fractionation calibration of Sharp et al. (1). (*B*) Diagenetic peak temperatures from Raman spectroscopy of carbonaceous matter (40) shown versus the calculated detrital aluminosilicate content (error bar: 90% prediction interval). $\delta^{18}O$ of authigenic quartz increases with increasing detrital aluminosilicate content at constant peak temperature.

of the three SiO_2 phases, the diffusion coefficients for porewater dissolved Si, and thus the thermodynamic driving force for any given reaction. The model includes the acceleration of the opal-CT to quartz transition with increasing detrital mineral fraction, which is empirically calibrated against the Lijiatuo section data (*SI Appendix*, Supporting Information 2), and successfully reproduces the quartz precipitation depth and $\delta^{18}O_{chert}$ values in Sea of Japan sediment cores (27).

Our model demonstrates that the fundamental control on the offset between $\delta^{18}O_{chert}$ and $\delta^{18}O_{SW}$ is the temperature window over which quartz precipitates and that this temperature is partially decoupled from seawater temperature. There is not one single temperature or depth at which opal-CT transforms to quartz (32). Rather, it depends on the suite of parameters that control the rate of progression along the entire SiO_2 diagenetic pathway that variably influence $\delta^{18}O_{chert}$ (Fig. 3). The model reveals that ambient pore fluid $\delta^{18}O$ is largely fluid-buffered, and hence, variation in water–rock ratios is not an important driver of $\delta^{18}O_{chert}$. Remarkably, heat flow (Q, W m^{-2}) has substantial leverage on $\delta^{18}O_{chert}$ (Fig. 3*B*), which means that $\delta^{18}O_{chert}$ paleothermometry must account for paleo heat flow. Model sensitivity analyses indicate that besides heat flow, $\delta^{18}O_{SW}$, and the decoupled T_{SW} effect, other parameters have little leverage over the secular trend in $\delta^{18}O_{chert}$ (*SI Appendix*, Supporting Information 3). Below, we show that the heat flow effect reconciles the early Paleozoic $\delta^{18}O_{chert}$ with only moderately depleted $\delta^{18}O_{SW}$ and moderate seawater temperatures and that low Archean $\delta^{18}O_{chert}$ requires neither high ocean temperatures nor very low $\delta^{18}O_{SW}$, given reasonable estimates of paleo heat flow.

Discussion

Impact of Heat Flow on $\delta^{18}O_{chert}$ and Seawater Temperature Reconstructions. Heat flow through ocean crust in the Phanerozoic can be quantified due to the well-established decrease in heat flow with crustal age (42) and the availability of reconstructions of crustal age distributions through time (43). In contrast with Precambrian time, most Phanerozoic chert forms in deep ocean settings. The average ocean crustal age in the early Paleozoic was ca. 20 Myr, increasing to ca. 50 Myr for the late Cenozoic (43). Applying the age–heat flow relationship (42) yields Paleozoic average heat flow values of ca. 105 mW m^{-2} and Cenozoic values of 80 mW m^{-2} (42). All else being equal, the heat flow effect from different ages of ocean crust alone accounts for ca. 2‰ of the 8‰ lower $\delta^{18}O_{chert}$ of Cambrian age relative to chert from the Eocene (Fig. 1). Considering heat flow thus solves the dilemma of $\delta^{18}O_{chert}$-inferred seawater temperatures above the metazoan lethal threshold without necessitating strongly ^{18}O-depleted oceans (44). Nonetheless, the lack of high $\delta^{18}O_{chert}$ values during the well-documented Paleozoic icehouses, combined with our demonstration of the insensitivity of $\delta^{18}O_{chert}$ to postprecipitation alteration, suggests that early Phanerozoic oceans were indeed moderately ^{18}O depleted.

Over longer timescales, a reduced sensitivity of $\delta^{18}O_{chert}$ to changes in T_{SW} precludes the hot Archean ocean hypothesis as the sole explanation for low $\delta^{18}O_{chert}$. A temperature reduction (ΔT_{SW}) from 70 to 5 °C at Archean heat flow yields an increase in $\delta^{18}O_{chert}$ of 9‰ (Fig. 3*C*) compared with 16‰ from direct application of the temperature–fractionation ($\varepsilon^{18/16}O$) relationship for the silica–water system. This behavior results from two mechanisms. First, the nonlinear relationship between $\varepsilon^{18/16}O$ and temperature (1) (*SI Appendix*, Fig. S7) means the same ΔT_{SW} translates to a smaller isotope difference at elevated diagenetic temperatures. Second, the offset between diagenetic temperatures and T_{SW} is reduced at higher T_{SW} (Fig. 3*A*), narrowing any given ΔT_{SW}.

Plausible decreases in heat flow explain a large fraction of the 15‰ $\delta^{18}O_{chert}$ increase across Earth history. Although detailed tectonic reconstructions are lacking for most of the Precambrian, diverse lines of evidence indicate that heat flow through Archean crust was around 2× higher (45–47) than the modern value of ca. 80 mW m^{-2} (42,45,48,49). A decrease of heat flow from 160 to 80 mW m^{-2} corresponds to an increase in $\delta^{18}O_{chert}$ of ca. 5.4‰ at T_{SW} = 5 °C, of 3.3‰ at T_{SW} = 30 °C, and of 1.3‰ at T_{SW} = 70 °C (Fig. 3 *A* and *C*). This control emerges from the kinetics of silica diagenesis: at lower heat flow, the opal-CT/quartz transformation happens later in time and at greater depth but at a lower temperature and thus with a larger silica–water fractionation (Fig. 3*A*). The heat flow effect on $\delta^{18}O_{chert}$ was previously overlooked and removes the requirement for extreme changes in $\delta^{18}O_{sw}$ to explain ^{18}O-depleted cherts, pointing the way toward a middle-ground scenario that satisfies all biological, geochemical, and paleoclimatological constraints without invoking pervasive alteration.

A 2× decrease in heat flow, in combination with either no temperature change or temperature reductions of 25 °C or 65 °C, produces shifts in $\delta^{18}O_{chert}$ of ca. 5, 10, or 14‰, respectively (Fig. 3*D*). Since we discount metamorphic or meteoric alteration, $\delta^{18}O_{SW}$ is the sole remaining explanation for the residual shift in the $\delta^{18}O_{chert}$ record (−10, −5, and −1‰, respectively). Thus, the scenario of hot Archean oceans with near-modern $\delta^{18}O_{sw}$ (50) can be mathematically salvaged if considered in conjunction with a ≥2× decrease in heat flow, but it remains biologically implausible and inconsistent with Precambrian glaciations. Beyond this, it is

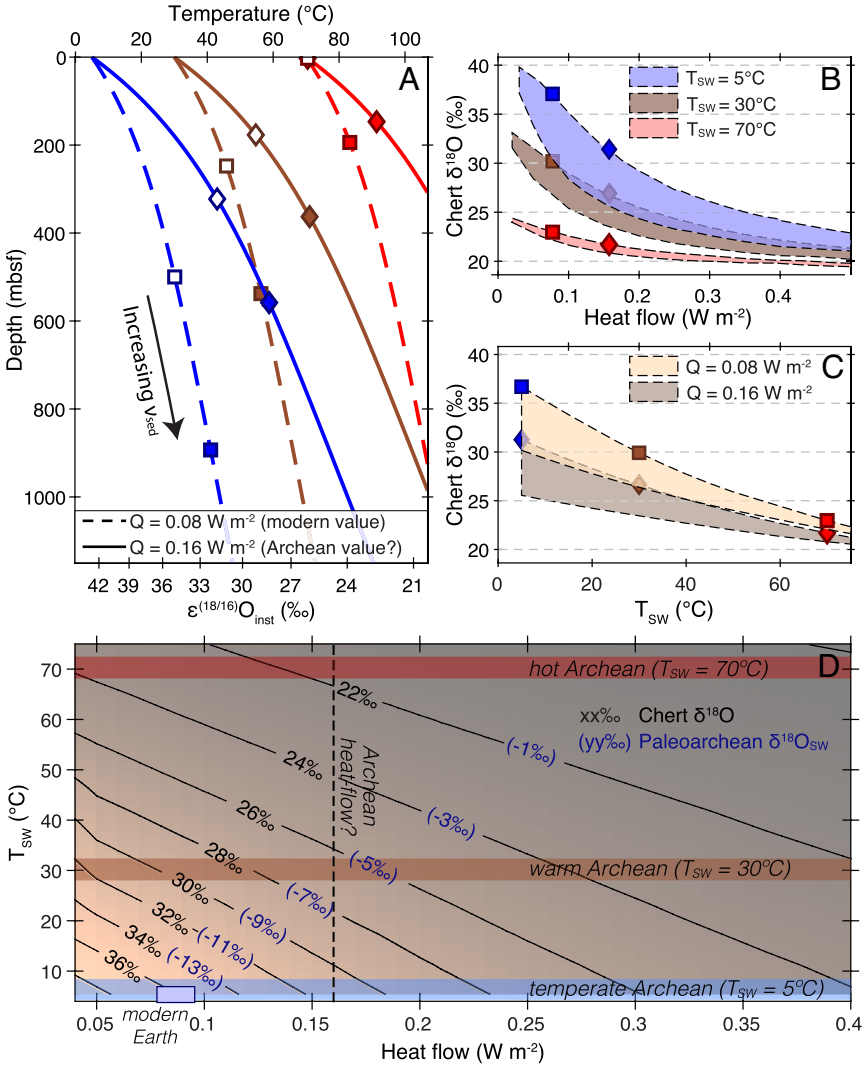

Fig. 3. Sensitivity of $\delta^{18}O_{chert}$ to bottom water temperature, heat flow, and sedimentation rate. Panel *A* shows six representative T–t paths for continental margin sediments produced by the combinations of 5 °C (blue lines; modern value), 30 °C (brown lines; warm Archean scenario), and 70 °C (red lines; hot Archean scenario) bottom water temperatures and heat flows of 80 mW m^{-2} (dashed lines; modern value) and 160 mW m^{-2} (solid lines; Archean estimate). Symbols plotting on the lines represent the modeled temperature (upper axis) and instantaneous oxygen isotope fractionation $\varepsilon^{(18/16)}O$ (lower axis) at the depth at which >99% of solid silica is present as quartz for moderate (100 m Myr^{-1}; filled symbols) and low (10 m Myr^{-1}; open symbols) sedimentation rates. Bottom water temperature, heat flow, and sedimentation rate all influence the depth, temperature, and oxygen isotope fractionation associated with quartz precipitation by altering the temperature–time diagenetic pathway silica follows as it is progressively buried. *B*: The isolated effect of heat flow for the three T_{SW} scenarios at constant v_{sed} of 100 m Myr^{-1}. *C*: The isolated effect of T_{SW} for two heat flow scenarios at constant v_{sed} of 100 m Myr^{-1}. Shaded areas in *B* and *C* show the range of model results encapsulated by parameterizations of three different depositional settings (continental margin, shelf, and abyss; *Materials and Methods*; "margin" parameterizations define the upper boundary and "abyss" parameterizations the lower boundary of the arrays); symbols correspond to scenarios in panel A and plot along the arrays defined by margin sediment. *D*: Combined influence of heat flow and T_{SW} on $\delta^{18}O_{chert}$, with temperate (5 °C, i.e., equivalent to modern-day bottom water temperature), warm (30 °C, after ref. (41)), and hot (70 °C, after refs. 5 and 9) Archean climate scenarios indicated by horizontal shading. Contours indicate modeled $\delta^{18}O_{chert}$ for the heat flow–T_{SW} combinations with modern $\delta^{18}O_{SW}$, with blue values in parentheses indicating what the Paleoarchean $\delta^{18}O_{SW}$ must have been to produce chert ca. 15‰ lower than the Cenozoic (Fig. 1) for a given T_{SW}–heat flow combination.

also incompatible with relatively constant $\delta^{18}O_{chert}$ ranges (cf. box-and-whisker plots in Fig. 1). Our model predicts that for a ΔT_{SW} of 65 °C (from 70 °C to 5 °C), the $\delta^{18}O_{chert}$ range should substantially increase (Fig. 3*C*). This behavior results from silica diagenesis occurring rapidly, at shallow depths, in all high-T_{SW} scenarios regardless of local heat flow, depositional setting, or sediment properties. Conversely, at lower $T_{SW,}$ the leverage of local variations in these properties on the overall silica transformation rate is increased, producing a broader distribution of $\delta^{18}O_{chert}$. We thus infer that the consistency in the range of $\delta^{18}O_{chert}$ through time is evidence for consistency in $T_{SW.}$

The seawater ^{18}O budget is itself a function of solid Earth dynamics (51, 52) and reflects the global ratio of high-T to low-T alteration processes. High-temperature hydrothermal fluids are the dominant source for ^{18}O because equilibrated fluids are close to a basalt $\delta^{18}O$ value of ca. 5.8‰. In contrast, low-T alteration products (e.g., clays) preferentially remove ^{18}O from the hydrosphere. The connection between the seawater ^{18}O budget and solid Earth dynamics thus arises by changing the high-T to low-T alteration ratio (14, 51). This can be achieved by altering parameters including crustal spreading rates or CO_2 degassing rates, the rate of continental emergence, plate tectonic regime, or global sea level. All these factors are known to influence the rate and temperature of oxygen-exchanging water–rock interactions (12, 14, 51). A recent numerical model that explicitly links the fluxes of ^{18}O to and from the hydrosphere with the thermal evolution of the solid Earth (52) suggests seawater $\delta^{18}O$ at 3.0 Ga of ca. 5 to 10‰ lower than today. These model predictions combine with the 1.3 to 5.4‰ decrease in $\delta^{18}O_{chert}$ resulting from

a 2× higher Archean heat flow (see above) to potentially explain essentially the entirety of the chert oxygen isotope record (Fig. 1). At a minimum, the thermal effects on $\delta^{18}O_{chert}$ sum to at least ca. 6.3‰, such that Archean seawater temperatures >30 °C are precluded (Fig. 3*D*). Overall, we conceptualize that $\delta^{18}O_{chert}$ encodes a dampened T_{SW} signal and both direct (heat flow) and indirect ($\delta^{18}O_{sw}$) effects of Earth's thermal evolution.

There are also controls over the ^{18}O fluxes that do not directly reflect solid Earth dynamics. More efficient reverse weathering reactions—the result of a high Precambrian ocean Si inventory (53)—would act to increase ^{18}O consumption directly by low-temperature mineral precipitation but also indirectly by increasing the net rate of continental silicate weathering—itself an ^{18}O consuming reaction—that has declined through time according to geochemical models (53,54). The continental surface has become gradually more covered by higher $\delta^{18}O$ sedimentary lithologies (55) with less leverage over the ocean ^{18}O seawater budget. Declining rates of reverse weathering and increasing continental sedimentary coverage thus both act to raise $\delta^{18}O_{SW}$ through time. Overall, we infer that a changing balance between high-T and low-T water–rock interactions through time has increased $\delta^{18}O_{SW}$ by up to 9‰ with the precise number depending on the Archean climate scenario. By accounting for heat flow, we are able to identify a compromise solution to the long-standing $T_{SW}/\delta^{18}O_{SW}$ debate, without having to invoke ubiquitous alteration or fortuitously monotonic climate evolution.

We show that the $\delta^{18}O_{chert}$ record is a largely pristine record of diagenetic conditions and is sensitive to heat flow. This finding implies that the long-term, near-monotonic increase in $\delta^{18}O_{chert}$ is an expression of Earth's thermal evolution. Accounting for heat flow helps explain the ^{18}O-depleted early Phanerozoic and Archean record without needing to invoke implausibly hot seawater or radically different $\delta^{18}O_{sw}$. We show that ca. 5‰ of the 15‰ Archean-Cenozoic difference in $\delta^{18}O_{chert}$ is directly attributable to a change in diagenetic temperatures caused by decreasing basal heat flow and in situ crustal heat production (Fig. 3). This effect combined with moderately depleted $\delta^{18}O_{sw}$ of ca. −5 to −9‰—in line with a recent $\delta^{18}O_{sw}$ evolution model explicitly forced by reconstructions of Earth's crustal and thermal evolution (52)—reconciles the chert $\delta^{18}O$ record with geological evidence for "icehouse" periods and high CO_2 sequestration fluxes in the late Archean (22). Geographic variation in seawater temperatures, chert depositional environments, sedimentation rates, and variations in detrital mineral contents contribute to the $\delta^{18}O_{chert}$ scatter at any given time. Seawater temperatures leave only a dampened signal in the record of $\delta^{18}O_{chert}$.

The framework we advance here is applicable to the oxygen isotope records of carbonates and other chemical sediments that recrystallize (i.e., undergo dissolution–reprecipitation reactions) or otherwise exchange with pore fluids during diagenesis. For example, foraminiferal tests have been shown to equilibrate their $\delta^{18}O$ with pore fluids at elevated temperatures during burial (56, 57). Since the extent of recrystallization and exchange are dependent on temperature and time, the $\delta^{18}O$ of other chemical sediments will also respond to changes in heat flow, although they will need specifically tailored assessments of their diagenetic pathways to fully exploit. Broadly, the similarity of $\delta^{18}O$ among carbonates, cherts, and other archives through geological time (13, 14) implies similar sensitivities to declining heat flow. Our framework also hints at future directions for empirical paleoclimate reconstructions when constraints on paleo heat flow and $\delta^{18}O_{sw}$ are available. Overall, the records of $\delta^{18}O$ from chemical sediments are strongly suggestive of a system driven by forcings that vary on billion-year timescales. Declining heat flow and increasing $\delta^{18}O_{sw}$ as the Earth cools provide such a driver in a way that the more capricious climate system cannot.

Materials and Methods

Analytical Methods. We analyzed cherts and silicified shales from the "Lijiatuo" section (28°24.519 N and 110°27.926 E) on the Yangtze Platform, China. We determined major element concentrations on fused bulk rock samples by X-ray fluorescence (XRF) with a Philips Panalytical PW2400. Sample X-ray diffraction (XRD) patterns were generated with a Panalytical Empyrean, and mineral phase composition and quantification were evaluated using Autoquan. The total organic carbon content (TOC) was determined on decarbonated samples (20% HCl) using an NA1500 elemental analyzer. Oxygen isotope ratios of bulk rocks were determined by laser fluorination gas source mass spectrometry (58), in which oxygen is liberated from samples in the presence of 10 mbar F_2 with a SYNRAD 50 W CO_2 laser. O_2 is purified from other reaction products in a series of liquid nitrogen cold traps and molecular sieves and ultimately introduced in continuous flow mode into a Thermo MAT 253 mass spectrometer. Oxygen isotopes were simultaneously measured on m/z = 32 ($^{16}O^{16}O$) and m/z = 34 ($^{16}O^{18}O$) for samples and the NIST NBS 28 standard and are reported as δ values on the VSMOW scale. In situ analyses of quartz grains was performed in epoxy-embedded samples using a Cameca 1280-HR SIMS with a primary $^{133}Cs^+$ beam to sputter O-ions. A low-energy electron gun was used to minimize surface charge accumulation. NIST NBS 28 ($\delta^{18}O_{VSMOW}$ = +9.57±0.10] was used to correct for instrumental mass bias and anchor the oxygen isotope ratios to the VSMOW scale. Results have an estimated reproducibility of ±0.35‰. Raman spectra of carbonaceous material were acquired using a Horiba Jobin Yvon HR800-UV spectrometer connected to an Olympus BX41 microscope operating in 180° backscattering geometry using a 488-nm Ar^+ laser for excitation. On-sample laser power was attenuated by density filters to <0.5 mW. Calibration of Raman bands was achieved using the 520.4 cm^{-1} silicon band, and spectra converted to an estimate of peak diagenetic temperature based on a temperature-dependent change in position and width of Raman bands in the first-order region of carbonaceous matter Raman spectra.

Siliceous Shale Authigenic Quartz $\delta^{18}O$. $\delta^{18}O$ values of authigenic quartz were derived by mass balance, assuming the bulk rock composition can be treated as a three-component mixing problem. We use measured $\delta^{18}O$ of bulk rock, prescribed detrital quartz and clay $\delta^{18}O$ values, typical shale clay/detrital quartz ratios, and measured Al concentrations to estimate the fraction of oxygen in authigenic quartz and its $\delta^{18}O$ value (all data given in *SI Appendix*, Supporting Information 4). This approach assumes clay minerals–dominated by illite–are the primary Al host, an assumption validated by the XRD spectra (*SI Appendix*, Supporting Information 1).

Chert $\delta^{18}O$ Compilation. We present the most comprehensive chert $\delta^{18}O$ compilation to date (Fig. 1 and *SI Appendix*, Supporting Information 5). Some anomalously low $\delta^{18}O$-values in Archean cherts are unlikely to be explained by sediment advection along geothermal gradients but by a different mode of formation. For instance, cherts interbedded in volcanic rocks were subject to locally very high temperatures (2), and narrow microscale $\delta^{18}O$ distributions likely reflect the reequilibration of $\delta^{18}O$ during hydrothermal alteration at 200 to 300 °C (59). In these cases, low $\delta^{18}O$ values do not represent the integrated t–T path during burial diagenesis. We have screened the database to include only sedimentary chert and omit silicified protoliths and vein mineralizations of SiO_2.

Chert Diagenesis Model. We have developed a 1D reaction–advection–diffusion model for silica diagenesis in marine sediments. The model tracks 12 independent mass balances (^{16}O, ^{18}O, and Si in four phases: opal-A, opal-CT, quartz, and porewater). Temperatures at each depth are defined from the heat flow and the geometric mean of water and sediment thermal conductivities and are subsequently used to define water–silica oxygen isotope fractionation factors, silica polymorph solubilities, diffusion coefficients, and silica polymorph dissolution and precipitation rate constants. Temperature profiles are dependent on sediment thermal conductivities, porosities, and compaction length scale, so we investigate three depositional settings (margin, shelf, and abyss) using typical values for these parameters in each setting from ref. (60). The model is run for each ensemble of input parameters until a depth is reached at which >99.99% of silica is present as quartz, and $\delta^{18}O_{quartz}$ has achieved a stable value. Once other local processes affecting porewater $\delta^{18}O$ are accounted for, the model successfully produces the depth of precipitation and $\delta^{18}O$ of authigenic quartz in Sea of Japan ODP cores 795 and 799 (27). Our

base model parameterization considers sediment thermal conductivity λ_s = 2.5 W m^{-1} K^{-1}, initial porosity ϕ_0 = 0.74, sediment compaction length scale $c = 1.7 \times 10^{-3}$ m^{-1}, sedimentation rate = 100 m Myr^{-1}, bottom water temperature = 25 °C, bottom water dissolved Si concentration = 100 μM L^{-1}, and detrital aluminosilicate mass fraction f_{sil} = 0.05. Unless specified, all results assume a modern average heat flow of 80 mW m^{-2}. All further parameters and constants are given in *SI Appendix*, Supporting Material 2.

Code Availability. All data and code required to reproduce the results shown in this manuscript are available through the GFZ Data Services at https://doi.org/10.5880/GFZ.3.3.2022.006.

ACKNOWLEDGMENTS. We thank the Deutsche Forschungsgemeinschaft (DFG) for funding MTs PhD (grant no. BL 562/11-2) that initiated this work and support of Friedhelm von Blanckenburg and the members of the Helmholtz Laboratory for the Geochemistry of the Earth Surface (HELGES) at GFZ Potsdam. P.J.F. acknowledges funding from the Swedish Research Council (VR #2015-06419) and support of the Topic Innovation Fund of the GFZ Potsdam. Frédéric Couffignal provided key support during the acquisition of SIMS data. We thank the members of the GFZ Geodynamics group for discussions and two anonymous reviewers for their comments on the manuscript.

Author affiliations: [a]Department of Sedimentology and Environmental Geology, Geoscience Center Georg-August-Universität Göttingen, 37077 Göttingen, Germany; [b]Earth Surface Geochemistry, GFZ German Research Centre for Geosciences, 14473 Potsdam, Germany; [c]Plants and Ecosystems (PLECO), Department of Biology, University of Antwerp, 2610 Wilrijk, Belgium; [d]Bundesanstalt für Materialforschung und –prüfung, 12489 Berlin, Germany; [e]Institut für Geologie und Mineralogie, Universität zu Köln, 50674 Cologne, Germany; and [f]Inorganic and Isotope Geochemistry, GFZ German Research Centre for Geosciences, 14473 Potsdam, Germany

1. Z. D. Sharp *et al.*, A calibration of the triple oxygen isotope fractionation in the SiO2-H2O system and applications to natural samples. *Geochim. Cosmochim. Acta* **186**, 105–119 (2016).
2. L. P. Knauth, D. R. Lowe, High Archean climatic temperature inferred from oxygen isotope geochemistry of cherts in the 3.5 Ga Swaziland Supergroup, South Africa. *Geol. Soc. Am. Bull.* **115**, 566–580 (2003).
3. L. P. Knauth, D. R. Lowe, Oxygen isotope geochemistry of cherts from the Onverwacht Group (3.4 Billion years), Transvaal, South Africa, with implications for secular variations in the isotopic composition of cherts. *Earth Planet. Sci. Lett.* **41**, 209–222 (1978).
4. F. Robert, M. Chaussidon, A palaeotemperature curve for the Precambrian oceans based on silicon isotopes in cherts. *Nature* **443**, 969–972 (2006).
5. L. P. Knauth, Temperature and salinity history of the Precambrian ocean: Implications for the course of microbial evolution. *Palaeogeogr. Palaeoclimatol. Palaeoecol.* **219**, 53–69 (2005).
6. Y. Kolodny, S. Epstein, Stable isotope geochemistry of deep sea cherts. *Geochim. Cosmochim. Acta* **40**, 1195–1209 (1976).
7. J. Marin-Carbonne, F. Robert, M. Chaussidon, The silicon and oxygen isotope compositions of Precambrian cherts: A record of oceanic paleo-temperatures? *Precambrian Res.* **247**, 223–234 (2014).
8. L. P. Knauth, S. Epstein, Hydrogen and oxygen isotope ratios in nodular and bedded cherts. *Geochim. Cosmochim. Acta* **40**, 1095–1108 (1976).
9. D. R. Lowe, D. E. Ibarra, N. Drabon, C. P. Chamberlain, Constraints on surface temperature 3.4 billion years ago based on triple oxygen isotopes of cherts from the Barberton Greenstone Belt, South Africa, and the problem of sample selection. *Am. J. Sci.* **320**, 790–814 (2020).
10. T. D. Brock, Life at high temperatures. *Science* **230**, 132–138 (1985).
11. J. M. Bennett *et al.*, The evolution of critical thermal limits of life on Earth. *Nat. Commun.* **12**, 1–9 (2021).
12. J. B. D. Jaffrés, G. A. Shields-Zhou, K. Wallmann, The oxygen isotope evolution of seawater: A critical review of a long-standing controversy and an improved geological water cycle model for the past 3.4 billion years. *Earth Sci. Rev.* **83**, 83–122 (2007).
13. N. Galili, The geologic history of seawater oxygen isotopes from marine iron oxides. *Science* **473**, 469–473 (2019).
14. J. F. Kasting *et al.*, Paleoclimates, ocean depth, and the oxygen isotopic composition of seawater. *Earth Planet. Sci. Lett.* **252**, 82–93 (2006).
15. J. Veizer, A. Prokoph, Temperatures and oxygen isotopic composition of Phanerozoic oceans. *Earth Sci. Rev.* **146**, 92–104 (2015).
16. U. Ryb, J. M. Eiler, Oxygen isotope composition of the Phanerozoic ocean and a possible solution to the dolomite problem. *Proc. Natl. Acad. Sci. U.S.A.* **115**, 6602–6607 (2018).
17. J. A. G. Wostbrock *et al.*, Calibration of carbonate-water triple oxygen isotope fractionation: Seeing through diagenesis in ancient carbonates. *Geochim. Cosmochim. Acta* **288**, 369–388 (2020).
18. E. C. Pope, D. K. Bird, M. T. Rosing, Isotope composition and volume of Earth's early oceans. *Proc. Natl. Acad. Sci. U.S.A.* **109**, 4371–4376 (2012).
19. R. T. Gregory, H. P. Taylor, An oxygen isotope profile in a section of Cretaceous oceanic crust, Samail Ophiolite, Oman: Evidence for δ 18 O buffering of the oceans by deep (>5 km) seawater-hydrothermal circulation at mid-ocean ridges. *J. Geophys. Res. Solid Earth* **86**, 2737–2755 (1981).
20. K. Muehlenbachs, R. N. Clayton, Oxygen isotope composition of the oceanic crust and its bearing on seawater. *J. Geophys. Res.* **81**, 4365 (1976).
21. D. O. Zakharov, I. N. Bindeman, Triple oxygen and hydrogen isotopic study of hydrothermally altered rocks from the 2.43–2.41 Ga Vetreny belt, Russia: An insight into the early Paleoproterozoic seawater. *Geochim. Cosmochim. Acta* **248**, 185–209 (2019).
22. D. Herwartz, A. Pack, T. J. Nagel, A CO2 greenhouse efficiently warmed the early Earth and decreased seawater 18O/16O before the onset of plate tectonics. *Proc. Natl. Acad. Sci. U.S.A.* **118**, e2023617118 (2021).
23. E. T. Degens, S. Epstein, Relationship between O18/O16 ratios in coexisting carbonates, cherts, and diatomites. *Am. Assoc. Pet. Geol. Bull.* **46**, 534–542 (1962).
24. S. Sengupta, A. Pack, Triple oxygen isotope mass balance for the Earth's oceans with application to Archean cherts. *Chem. Geol.* **495**, 18–26 (2018).
25. F. L. Liljestrand *et al.*, The triple oxygen isotope composition of Precambrian chert. *Earth Planet. Sci. Lett.* **537**, 116167 (2020).
26. D. E. Ibarra *et al.*, Triple oxygen isotope systematics of diagenetic recrystallization of diatom opal-A to opal-CT to microquartz in deep sea sediments. *Geochim. Cosmochim. Acta*, 10.1016/j.gca.2021.11.027 (2021).
27. A. G. Yanchilina, R. Yam, Y. Kolodny, A. Shemesh, From diatom opal-A δ18O to chert δ18O in deep sea sediments. *Geochim. Cosmochim. Acta* **268**, 368–382 (2020).
28. L. A. Williams, G. A. Parks, D. A. Crerar, Silica diagenesis, I. solubility controls. *J. Sediment. Petrol.* **55**, 301–311 (1985).
29. S. Varkouhi, N. J. Tosca, J. A. Cartwright, Temperature–time relationships and their implications for thermal history and modelling of silica diagenesis in deep-sea sediments. *Mar. Geol.* **439**, 106541 (2021).
30. K. J. Murata, I. Friedman, J. D. Gleason, Oxygen isotope relations between diagenetic silica minerals in Monterey Shale, Temblor Range, California. *Am. J. Sci.* **277**, 259–272 (1977).
31. J. R. Farver, R. A. Yund, Oxygen diffusion in quartz: Dependence on temperature and water fugacity. *Chem. Geol.* **90**, 55–70 (1991).
32. K. A. Pisciotto, Diagenetic trends in the siliceous facies of the Monterey Shale in the Santa Maria region, California. *Sedimentology* **28**, 547–571 (1981).
33. S. Mizutani, Progressive ordering of cristobalitic silica in the early stage of diagenesis. *Contrib. Mineral. Petrol.* **61**, 129–140 (1977).
34. C. M. Isaacs, Influence of rock composition on kinetics of silica phase changes in the monterey formation, Santa Barbara area, California. *Geology* **10**, 304 (1982).
35. N. W. Hinman, Chemical factors influencing the rates and sequences of silica phase transitions: Effects of organic constituents. *Geochim. Cosmochim. Acta* **54**, 1563–1574 (1990).
36. M. Kastner, J. B. Keene, J. M. Gieskes, Diagenesis of siliceous oozes-I. Chemical controls on the rate of opal-A to opal-CT transformation- an experimental study. *Geochim. Cosmochim. Acta* **41**, 1041–1059 (1977).
37. S. Dixit, P. Van Cappellen, A. J. van Bennekom, Processes controlling solubility of biogenic silica and pore water build-up of silicic acid in marine sediments. *Mar. Chem.* **73**, 333–352 (2001).
38. P. Van Cappellen, L. Qiu, Biogenic silica dissolution in sediments of the Southern Ocean. I. Solubility. *Deep. Res. II* **44**, 1109–1128 (1997).
39. M. Tatzel, F. von Blanckenburg, M. Oelze, J. Bouchez, D. Hippler, Late Neoproterozoic seawater oxygenation by siliceous sponges. *Nat. Commun.* **8**, 621 (2017).
40. N. K. Lünsdorf, I. Dunkl, B. C. Schmidt, G. Rantitsch, H. von Eynatten, Towards a higher comparability of geothermometric data obtained by Raman spectroscopy of carbonaceous material. Part 2: A revised geothermometer. *Geostand. Geoanalytical Res.* **41**, 593–612 (2017), 10.1111/ggr.12178.
41. R. E. Blake, S. J. Chang, A. Lepland, Phosphate oxygen isotopic evidence for a temperate and biologically active Archaean ocean. *Nature* **464**, 1029–1032 (2010).
42. D. Hasterok, D. S. Chapman, E. E. Davis, Oceanic heat flow: Implications for global heat loss. *Earth Planet. Sci. Lett.* **311**, 386–395 (2011).
43. C. Vérard, C. Hochard, P. O. Baumgartner, G. M. Stampfli, M. Liu, Geodynamic evolution of the Earth over the phanerozoic: Plate tectonic activity and palaeoclimatic indicators. *J. Palaeogeogr.* **4**, 167–188 (2015).
44. T. W. Hearing *et al.*, An early Cambrian greenhouse climate. *Sci. Adv.* **4**, 1–12 (2018).
45. T. Nakagawa, P. J. Tackley, Influence of plate tectonic mode on the coupled thermochemical evolution of Earth's mantle and core. *Geochem. Geophys. Geosyst.* **16**, 3400–3413 (2015).
46. M. P. Ptáček, N. Dauphas, N. D. Greber, Chemical evolution of the continental crust from a data-driven inversion of terrigenous sediment compositions. *Earth Planet. Sci. Lett.* **539**, 116090 (2020).
47. T. M. Harrison, The Hadean crust: Evidence from >4 Ga Zircons. *Annu. Rev. Earth Planet. Sci.* **37**, 479–505 (2009).
48. C. Jaupart, J. C. Mareschal, "Constraints on crustal heat production from heat flow data" in *Treatise on Geochemistry*, H. D. Holland, K. K. Turekian, Eds. (Elsevier Ltd., ed. 2, 2014), pp. 53–73.
49. J. G. Sclater, C. Jaupart, D. Galson, The heat flow through Oceanic and Continental crust and the heat loss of the Earth. *Rev. Geophys.* **18**, 269–311 (1980).
50. J. P. McGunnigle *et al.*, Triple oxygen isotope evidence for a hot Archean ocean. *Geology* **50**, 991–995 (2022).
51. C. Vérard, J. Veizer, On plate tectonics and ocean temperatures. *Geology* **47**, 882–885 (2019).
52. M. Guo, J. A. G. Wostbrock, N. J. Planavsky, J. Korenaga, Reconstructing seawater δ 18 O and system evolution O values with solid Earth. *Earth Planet. Sci. Lett.* **592**, 117637 (2022).
53. J. Krissansen-Totton, D. C. Catling, A coupled carbon-silicon cycle model over Earth history: Reverse weathering as a possible explanation of a warm mid-Proterozoic climate. *Earth Planet. Sci. Lett.* **537**, 116181 (2020).
54. B. J. W. Mills, T. M. Lenton, A. J. Watson, Proterozoic oxygen rise linked to shifting balance between seafloor and terrestrial weathering. *Proc. Natl. Acad. Sci. U.S.A.* **111**, 9073–9078 (2014).

55. A. B. Ronov, General trends in the evolution of the composition of the crust, ocean and atmosphere. *Geokhimiya* **8**, 715–743 (1964).
56. S. Bernard, D. Daval, P. Ackerer, S. Pont, A. Meibom, Burial-induced oxygen-isotope re-equilibration of fossil foraminifera explains ocean paleotemperature paradoxes. *Nat. Commun.* **8**, 1–10 (2017).
57. J. S. Killingley, Effects of diagenetic recrystallization on 18O/16O values of deep-sea sediments. *Nature* **301**, 594–597 (1983).
58. Z. D. Sharp, A laser-based microanalytical method for the in situ determination of oxygen isotope ratios of silicates and oxides. *Geochim. Cosmochim. Acta* **54**, 1353–1357 (1990).
59. J. Marin-Carbonne, M. Chaussidon, M.-C. Boiron, F. Robert, A combined in situ oxygen, silicon isotopic and fluid inclusion study of a chert sample from Onverwacht Group (3.35Ga, South Africa): New constraints on fluid circulation. *Chem. Geol.* **286**, 59–71 (2011).
60. D. E. LaRowe, E. Burwicz, S. Arndt, A. W. Dale, J. P. Amend, Temperature and volume of global marine sediments. *Geology* **45**, 275–278 (2017).